

Ultrafast dynamics of the low frequency shear phonon in 1T'–MoTe₂

Takumi Fukuda,^{1,*} Kotaro Makino,² Yuta Saito,² Paul Fons,²
Alexander V. Kolobov,^{2,3} Keiji Ueno,⁴ and Muneaki Hase^{1,†}

¹*Department of Applied Physics, Graduate school of Pure and Applied Sciences,
University of Tsukuba, 1-1-1 Tennodai, Tsukuba 305-8573, Japan*

²*Nanoelectronics Research Institute, National Institute of Advanced Industrial Science and Technology (AIST),
Tsukuba Central 5, 1-1-1 Higashi, Tsukuba 305-8565, Japan*

³*Department of Physical Electronics, Faculty of Physics,
Herzen State Pedagogical University of Russia, 48 Moika Embankment, St. Petersburg, 191186, Russia*

⁴*Graduate School of Science and Engineering, Saitama University, Saitama 338-8570, Japan*

We report on the dynamics of coherent phonons in semimetal 1T'–MoTe₂ using femtosecond pump–probe spectroscopy. On an ultrafast sub–picosecond time scale at room temperature, a low frequency and long–lifetime shear phonon mode was observed at 0.39 THz, which was previously reported in the form of a characteristic phonon only in the low temperature T_d–MoTe₂ phase. Unlike the other optical phonon modes, the shear phonon mode was found to strongly couple with photoexcited carriers. Moreover, the amplitude of the shear mode surprisingly decreased with increasing excitation density, a phenomenon which can be attributed to be a consequence of the lattice temperature rising after excitation. These results provide useful physical information on ultrafast lattice symmetry switching between the normal semimetal 1T' and the lattice inversion symmetry breaking Type–II Weyl semimetal T_d phases.

Recent interest in transition metal dichalcogenides (TMDCs) has dramatically increased owing to the variety of unusual properties stemming from the existence of two dimensional Van der Waals (VdW) structures, such as graphene [1–3]. One of the reasons that drives research in TMDCs is that they intrinsically possess a wide variety of possible crystal and electronic structures depending on the large number of accessible chemical combinations between metal (Mo, W, ...) and chalcogen (S, Se, Te) atoms, as well as the accessibility of other phases by low energy photon excitation [4]. These versatile properties can be useful for further understanding of the fundamental properties of topological materials as well as the advancement of high-performance and functional electronic, optoelectronic and quantum devices [5–7], particularly the next generation of strain–engineered phase–change materials [8] or phase patterning technology driven by light [9]. Within the TMDC family, MoTe₂ has attracted considerable attention because of the presence of rich structural and electronic phases. MoTe₂ has three possible structural phases, the trigonal prismatic 2H semiconducting phase (the most stable at room temperature: RT), the centrosymmetric monoclinic 1T' semimetal phase (metastable at RT), and the lattice symmetry breaking orthorhombic T_d semimetal phase (stable below 250 K). Among these phases, the 1T' and T_d structures are similar, except for distortions along the *a*– or *b*–axes as shown in Fig.1(a) and (b). MoTe₂ is also known for being a candidate topological phase material such as a topological insulator (TI) or a Weyl semimetal (WSM) due to the breaking of lattice inversion symmetry by certain layer configurations. First-principle calculations and observations of Fermi arcs in lattice symmetry breaking orthorhombic T_d–MoTe₂ and similar structure, T_d–WTe₂, have led to the establishment and confirmation of the theory of Type–II WSMs with intriguing

carrier transport properties with unusually long lifetimes [10–14].

Very recently, some groups have observed the ultrafast dynamics of coherent phonons (CPs) and lattice symmetry switching between the 1T' and T_d phases, which corresponds to a phase transition from the WSM to the normal phases. Sie *et al.* induced shear displacements using THz pump pulses in the T_d phase of WTe₂, which was monitored by ultrafast electron diffraction [15]. Zhang *et al.*, on the other hand, observed a similar phenomenon using optical pump–probe reflectivity measurements from extremely low temperature 4K to near RT [16], corresponding to the low temperature T_d phase. However, the related CPs at RT of the 1T'–MoTe₂ phase have not been well investigated. Therefore it is still unclear if photoexcitation of the high temperature 1T' phase induces a phase transition in MoTe₂. It is important to gain insight into the photoexcited state at RT and even higher temperatures in TMDCs, because of potential device applications in general temperature conditions.

Here, we investigate the dynamics of CPs in monoclinic 1T'–MoTe₂ at RT using a femtosecond optical pump–probe reflectivity technique with a high signal to noise ratio. In addition to the typical Raman–active optical modes of the 1T' phase, a T_d–originated shear vibration mode is also clearly observed in the high temperature 1T' phase. The time–domain CP oscillations are analyzed using a short window Fourier transform method, which enables the extraction of the dynamics related to the generation and decay of each phonon mode in time–frequency space. Our results indicate that the light–induced structural phase transition between the adjacent 1T' and T_d phases, here referred to as "lattice symmetry switching", occurs even at RT. We suggest that the ultrafast dynamics of such switching is an important research subject necessary to explore the ap-

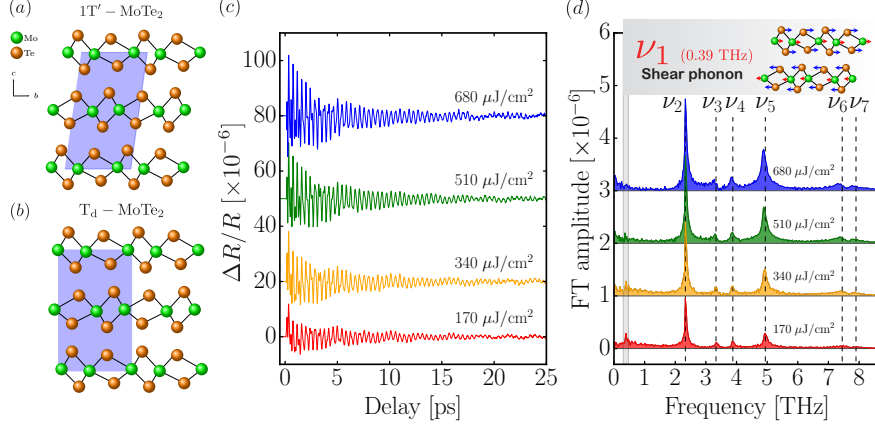


FIG. 1. (a) and (b) are the crystal structures of monoclinic 1T'-MoTe₂ and orthorhombic T_d - MoTe₂, respectively. The blue colored areas represent the unit cells. (c) Fluence dependent (170 to 680 $\mu\text{J}/\text{cm}^2$) time domain signals of CPs in 1T' phase obtained from the $\Delta R/R$ signal, where the excited carrier response has been subtracted as background. (d) FT amplitude spectra of (c) and a schematic image of the shear phonon of the ν_1 mode in inset.

plications of MoTe₂ as a Type-II WSM.

Optical pump-probe measurements were carried out using a Ti:sapphire oscillator operated at 80 MHz, which provided near infrared optical pulses with a pulse duration of ≤ 30 fs and a central wavelength of 830 nm (with a corresponding photon energy of $\hbar\omega \sim 1.5$ eV). It should be noted that the continuous heating effect by the 80 MHz repetition laser is negligibly small, as demonstrated by the phonon spectra shown below exhibiting the almost same peak positions as those of previous Raman studies on bulk 1T'-MoTe₂. The average fluence of the pump beam was varied from $F = 170$ to $680 \mu\text{J}/\text{cm}^2$. The upper limit of fluence ($680 \mu\text{J}/\text{cm}^2$) was set to prevent surface damage. The *s*-polarized pump and the *p*-polarized probe beams were co-focused onto the sample to a spot size of $\approx 8 \mu\text{m}$ with an incident angles of about 5° and 15° with respect to the sample normal, respectively. The optical penetration depth at 830 nm was estimated to be 50 nm from the complex dielectric function as calculated by density functional theory (DFT) simulations. The delay between the pump and probe pulses was scanned up to 30 ps [17] by an oscillating retroreflector operated at a frequency of 9.5 Hz. The transient reflectivity change ($\Delta R/R$) was recorded as a function of pump-probe time delay. The measurements were performed in air at RT. The figures used in this article were generated using Matplotlib [18].

The sample used was a small flake of a 1T'-MoTe₂ single crystal with the *c*-axis of the crystal corresponding to the sample normal. The 1T'-MoTe₂ bulk crystal was prepared by Chemical Vapor Transport [19]. The crystal thickness was $\geq 500 \mu\text{m}$ and strain and/or confinement effects were negligible [20]. In addition, Raman measurements on our 1T'-MoTe₂ sample indicated no peak at 13 cm^{-1} ($= 0.39 \text{ THz}$) and thus confirming that our sample at RT does not include the T_d phase.

Fig.1(c) shows the $\Delta R/R$ signals measured for the

1T'-MoTe₂ phase with sub-picosecond time resolution for a variety of pump fluences ranging from 170 to $680 \mu\text{J}/\text{cm}^2$. CP oscillations can be clearly observed up to ~ 25 ps time delay at RT. The oscillations are not simply sinusoidal, suggesting the existence of multiple phonon modes driven by charge-density fluctuations, which traditionally described by resonant impulsive stimulated Raman scattering (ISRS) [21, 22] or by a displacive excitation of CP (DECP) mechanism [23]. Under the condition that the pump photon is absorbed by an opaque sample, the driving force can be described by the Raman tensor, which includes both the resonant ISRS and DECP mechanisms. In the following we will briefly introduce the DECP mechanism. DECP theory describes that the initial phonon coordinate $Q_0(t)$ is proportional to the photoexcited carrier density $n(t)$, namely,

$$Q_0(t) = \kappa n(t), \quad (1)$$

where κ is a constant. Considering the relation $\Delta R(t)/R \propto Q_0$, the time evolution of phonon amplitude of CP generated by the DECP process should follow the dynamics of photoexcited carrier density $n(t)$.

Fig.1(d) shows the Fourier transformed (FT) spectra of the time domain CP signals for 1T'-MoTe₂ obtained for different pump fluences. According to the FT spectra, it can be seen that a total of seven different phonon modes can be observed in the $\Delta R/R$ data. Each of the phonon frequencies has been labeled as $\nu_1 \sim \nu_7$ from the lowest to the highest frequency. In detail, $\nu_1 = 0.39 \text{ THz}$, $\nu_2 = 2.34 \text{ THz}$, $\nu_3 = 3.34 \text{ THz}$, $\nu_4 = 3.88 \text{ THz}$, $\nu_5 = 4.94 \text{ THz}$, $\nu_6 = 7.48 \text{ THz}$ and $\nu_7 = 7.90 \text{ THz}$. In particular, $\nu_2 \sim \nu_7$ modes, which are observed by the present optical pump-probe method, are consistent with the Raman spectra of the 1T' phase at RT, as reported recently by various groups [24–27].

The low frequency ν_1 mode is, however, absent in the Raman spectra of the 1T' phase at RT, but is character-

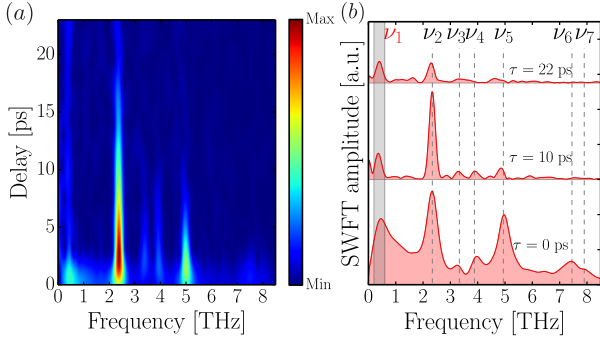


FIG. 2. (a) SWFT spectrogram of the $\Delta R/R$ signal for $F = 170 \mu\text{J}/\text{cm}^2$ of (a). The FT amplitude spectrum at $\tau = 0, 10, 22$ ps (in (a)) are displayed in (b).

istic of the T_d phase, which is a low temperature phase ($< 250\text{K}$) of MoTe_2 . Note that ν_1 can be assigned to the A_1 mode in the T_d phase or as the B_u mode in the $1T'$ phase, while the $\nu_2 \sim \nu_7$ phonon modes can be assigned as the A_1 modes in the T_d phase or as the A_g mode in the $1T'$ phase, according to previous reports [24, 25, 27]. It is generally impossible to observe an infrared-active B_u phonon mode in pump-probe measurements based on resonant ISRS or DECP processes [21–23]. This implies, in our experiments, the low frequency ν_1 mode cannot be the B_u mode of the $1T'$ phase. Thus, the low frequency ν_1 phonon observed in the present study is assigned to the A_1 mode originating from the T_d phase as discussed in detail below.

The low frequency ν_1 mode can be considered to be an interlayer shear vibration mode [15, 16], a mode that is a key to lattice symmetry switching [24, 25] as can be seen in the inset of Fig.1(d). It can also be seen that the asymmetric shape of the FT amplitude around ν_4 at low excitation density, as shown in Fig.1(d) at $F \leq 340 \mu\text{J}/\text{cm}^2$, implies the existence of a splitting of a phonon mode ($131 \text{ cm}^{-1} = 3.93 \text{ THz}$), which is also characteristic of the T_d phase. Thus, the fact that the low frequency ν_1 mode was observed even at RT suggests the possibility of a transient structural transition to the T_d phase or a mixture of the two competing $1T'$ and T_d phases upon photoexcitation. It was also noted, in the present study, that the $2H$ phase does not play a role in the structural phase transition.

Fig.2(a) shows a short window FT (SWFT) spectrogram [28] for $F = 170 \mu\text{J}/\text{cm}^2$, a time-frequency-domain representation of Fig.1(a). Here, the FWHM of the Gaussian window function was set as 2.0 ps to eliminate any artifacts due to edge effects while allowing the detection of the low ($< 0.5 \text{ THz}$) frequency ν_1 mode. The dominant optical phonon modes as well as the ν_1 mode can be seen, and they decay with dramatically different time constants. In particular, the lifetimes of the $\nu_3 \sim \nu_7$ modes were found to decay within several picoseconds, which is a typical behavior of CPs, however, the ν_1 and ν_2 modes

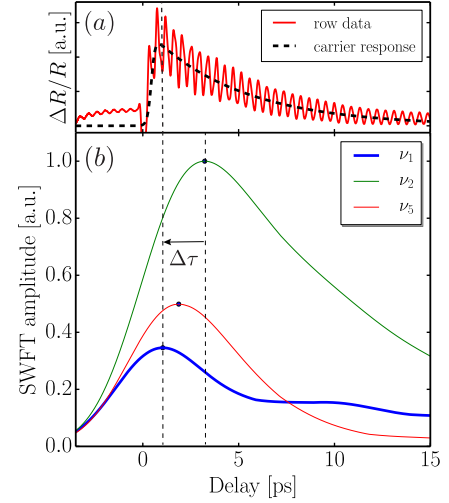


FIG. 3. (a) Part of $\Delta R/R$ signal including carrier relaxation and the phonon oscillations of $1T'$ phase at $170 \mu\text{J}/\text{cm}^2$. The dashed line represents the carrier relaxation in the signal. (b) Time evolution of the SWFT amplitudes for ν_1 , ν_2 , ν_5 modes as a function of the time delay. The vertical dashed lines represent the peak positions. $\Delta\tau$ represents the time lag between the ν_1 and ν_2 modes.

persisted beyond ≈ 22 ps up to the limit of the time delay of the measurement. To explore this in more detail, we performed a fit of the time-domain data for $F = 170 \mu\text{J}/\text{cm}^2$ shown in Fig.1(c) using damped oscillations with the three dominant frequencies ν_1 , ν_2 and ν_5 ,

$$\frac{\Delta R(t)}{R} = \sum_{i=1,2,5} \xi_i e^{-\frac{t}{\tau_i}} \cos(2\pi\nu_i t + \varphi_i), \quad (2)$$

where ξ_i is the amplitude, τ_i is the relaxation time, ν_i is the frequency and φ_i is the initial phase of the CP. The fit indicates $\tau_1 = 21.7 \pm 1.4$ ps, $\tau_2 = 9.8 \pm 0.04$ ps and $\tau_5 = 3.7 \pm 0.1$ ps. The ν_1 mode exhibits an even much longer lifetime than that of the ν_2 and ν_5 modes. It is noted that these relaxation times only weakly depend on the pump fluence, and therefore we will not discuss this effect here. The fit also indicates $\varphi_1 = 27 \pm 2^\circ$, $\varphi_2 = 90 \pm 1^\circ$, and $\varphi_5 = 96 \pm 1^\circ$. Considering the value of φ_1 obtained above, the initial phase of the ν_1 mode is found to be cosine-like, while the other modes, φ_2 and φ_5 ($\approx \pi/2$), exhibits sine-like behavior. It can also be seen that the shear vibration mode (ν_1) exhibits a larger amplitude than that observed in static spectra (Fig.1(d)) just after the excitation by the pump pulse ($\tau = 0$ ps) as seen in Fig.2(b).

Fig.3 shows the time evolution of the peak amplitude for the three dominant modes ν_1 , ν_2 , and ν_5 , shown in Fig.2(a). According to Fig.3(b), the rise time of the amplitude of the ν_1 mode is the fastest among all the vibrational modes (this is also the case for the other optical modes although the data is not shown) just after

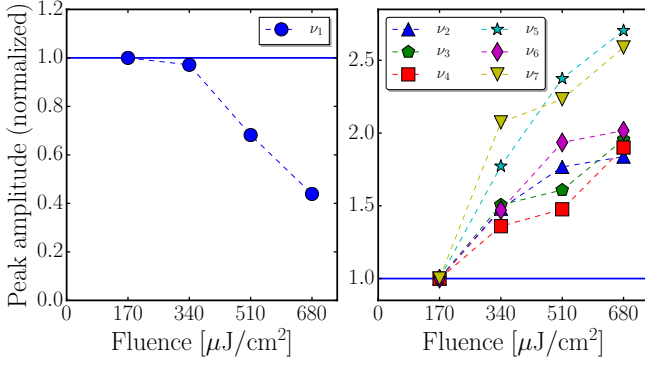


FIG. 4. Fluence dependent peak amplitude shifts normalized by each of the values for $F = 170 \mu\text{J}/\text{cm}^2$ for ν_1 (a) and $\nu_2 \sim \nu_7$ (b) obtained from the FT spectra displayed in Fig.1(d).

excitation. It was also found that the rise of the ν_1 mode coincides with that of the photoexcited carrier dynamics shown in Fig.3(a) in accordance with eq.(1). In addition to the results in Fig.3, the fact that the ν_1 mode exhibits dispersive behavior (cosine-like), while the other modes exhibit impulsive behavior (sine-like), indicates the ν_1 mode strongly couples with the photogenerated carriers and is excited preferentially over all the phonon modes. Thus, under low excitation density (170 $\mu\text{J}/\text{cm}^2$) in which the lattice temperature rise is negligibly small, photoexcited carriers exert a step function electrostrictive force on the lattice driving the coherent ν_1 mode, which induces the lattice symmetry of 1T' phase to partially change toward T_d phase.

Based on the relationship between the carrier (electron) relaxation time and the initial phase of the coherent phonons for simple semimetals (i.e., $\tan\varphi = \Gamma/\Omega$, where Γ is the reciprocal of carrier relaxation time and $\Omega = 2\pi\nu$) [23, 29], Fig.3 also suggests a different relaxation time as the driving force of three dominant phonon modes. That is the shorter the carrier relaxation time τ_{el} , the stronger the impulsive behavior (sine-like). In fact, the observation that the dispersive-like ν_1 mode strongly couples with photoexcited carriers, indicates a longer relaxation time on the order of several picoseconds (See Fig.3(a)), consistent with the relationship discussed. On the other hand, the other modes exhibit impulsive behavior (sine-like), and therefore the carrier relaxation time for the driving force coupled with these modes would be short lived, although more experimental and theoretical work is required to fully understand the different carrier dynamics in TMDC systems.

Fig.4 shows the peak amplitudes versus the pump fluence obtained from Fig.1(d), being plotted for the low frequency ν_1 mode in Fig.4(a) and for the other optical modes in Fig.4(b). First, for the $\nu_2 \sim \nu_7$ cases, Fig.4(b) shows that the peak intensities (amplitudes) almost linearly increase with increasing pump fluence. This phenomenon can be understood as a characteristic property of CPs, as observed for conventional semiconductors and

metals [30–32]. In contrast, the peak intensity of the ν_1 mode surprisingly decreased with increasing pump fluence, as seen in Fig.4(a). This behavior was opposite to that of the characteristic CP modes $\nu_2 \sim \nu_7$, suggesting that the ν_1 mode is sensitive to the lattice temperature (T_l) [24, 25], as very recently reported by Zhang, *et al.*[16]. Although the amplitude near time zero (ξ_1) increases with excitation fluence, the lattice temperature rise promotes faster dephasing of the coherent phonons, resulting in the decrease of FT amplitude as shown in Fig.4(a) [33, 34].

Comparing the measurements taken at ultra-low temperature ($T = 4 \text{ K}$) [16] and our present measurements at RT, the pump fluence dependence of the T_l is expected to be significantly different. In fact, the maximum pump fluence used by Zhang *et al.* was up to $\approx 5 \text{ mJ}/\text{cm}^2$, while in the current experiments was only 680 $\mu\text{J}/\text{cm}^2$, a fluence value one order less. Thus, the rise of T_l in the current study is also expected to be one order of magnitude less than in the former study. According to two-temperature model (TTM) calculations [35], the maximum increase in the T_l in the 1T'–MoTe₂ bulk crystal surface can be estimated to be from 305 K to 321 K, for pump fluences 170 to 680 $\mu\text{J}/\text{cm}^2$, where the initial temperature was set as $T_l = 300 \text{ K}$. This TTM calculation result shows the pump pulse irradiation results in a rise of $\Delta T_l \approx 20 \text{ K}$ at the sample surface. Although the phase transition between the 1T' and T_d phases has been believed to occur at 250 K, our data strongly suggest that the low frequency ν_1 phonon in the T_d phase appears upon photoexcitation even at RT. A possible mechanism for the light-induced structural phase transition from 1T to T_d phases is the transient displacement of the nuclear equilibrium position of the ν_1 mode, which is induced and stabilized by electron doping via photoexcitation, as has been recently proposed by Kim *et al.* [36]. The pump-induced temperature rise (ΔT_l) may partly contribute to the decrease in the peak amplitude [Fig.4(a)] since higher temperature will destroy the T_d phase [36]. The transient phase transition between the normal semimetal 1T' and the WSM T_d phases observed in the sub-picosecond time domain is expected to be a key phenomenon in controlling the process of the creation and annihilation of Weyl fermions and allows the development of ultrafast phase switching device applications at RT.

In conclusion, we observed a long lifetime low frequency shear phonon in the 1T'–MoTe₂ phase even at RT using pump-probe spectroscopy, which was thought to be present in only the T_d phase below 250 K. The observed behavior implies the existence of a transient phase transition from the normal semimetal 1T' phase to the Type-II WSM T_d phase or a mixture between both phases in the ultrafast sub-picosecond time domain. The SWFT analysis revealed that the amplitude of the shear phonon, which is considered to result in lattice symmetry breaking in the bulk crystal, is largely induced just after excitation, caused by a resonant ISRS or

DECP mechanism. High fluence laser irradiation leads the shear phonon mode to decrease in amplitude due to a lattice temperature rise of ≈ 20 K as calculated by a TTM analysis. This study on ultrafast dynamics in the 1T' phase is in agreement with the existence of previously reported lattice symmetry switching between the normal semimetal to the WSM phase even at RT, and also suggests a new technique to unveil the sub-picosecond time domain creation and annihilation of Weyl fermions as

well as their thermal dependence which is expected to lead to new device applications using topological phase switching.

This work was supported by JSPS KAKENHI (Grant Numbers. 17H02908 and 19H02619), and CREST, JST (Grant Number. JPMJCR1875), Japan. We gratefully acknowledge R. Mondal for helping data analysis, and R. Ishikawa, T. Mori at Saitama University for measuring Raman spectrum data of our 1T'–MoTe₂ sample.

* s1920338@s.tsukuba.ac.jp

† mhase@bk.tsukuba.ac.jp

- [1] K. S. Novoselov, A. K. Geim, S. V. Morozov, D. Jiang, Y. Zhang, S. V. Dubonos, I. V. Grigorieva, and A. A. Firsov, *Science* **306**, 666 (2004).
- [2] K. S. Novoselov, A. K. Geim, S. Morozov, D. Jiang, M. Katsnelson, I. Grigorieva, S. Dubonos, and A. A. Firsov, *Nature* **438**, 197 (2005).
- [3] A. K. Geim, *Science* **324**, 1530 (2009).
- [4] A. V. Kolobov, P. Fons, and J. Tominaga, *Phys. Rev. B* **94**, 094114 (2016).
- [5] D. Unuchek, A. Ciarrocchi, A. Avsar, K. Watanabe, T. Taniguchi, and A. Kis, *Nature* **560**, 340 (2018).
- [6] Q. H. Wang, K. Kalantar-Zadeh, A. Kis, J. N. Coleman, and M. S. Strano, *Nat. Nanotech.* **7**, 699 (2012).
- [7] M. Chhowalla, H. S. Shin, G. Eda, L.-J. Li, K. P. Loh, and H. Zhang, *Nat. Chem.* **5**, 263 (2013).
- [8] S. Song, D. H. Keum, S. Cho, D. Perello, Y. Kim, and Y. H. Lee, *Nano Lett.* **16**, 188 (2015).
- [9] S. Cho, S. Kim, J. H. Kim, J. Zhao, J. Seok, D. H. Keum, J. Baik, D.-H. Choe, K. J. Chang, K. Suenaga, S. W. Kim, Y. H. Lee, and H. Yang, *Science* **349**, 625 (2015).
- [10] A. A. Soluyanov, D. Gresch, Z. Wang, Q. Wu, M. Troyer, X. Dai, and B. A. Bernevig, *Nature* **527**, 495 (2015).
- [11] Y. Sun, S.-C. Wu, M. N. Ali, C. Felser, and B. Yan, *Phys. Rev. B* **92**, 161107 (2015).
- [12] L. Huang, T. M. McCormick, M. Ochi, Z. Zhao, M.-T. Suzuki, R. Arita, Y. Wu, D. Mou, H. Cao, J. Yan, N. Trivedi, and A. Kaminski, *Nat. Mater.* **15**, 1155 (2016).
- [13] K. Deng, G. Wan, P. Deng, K. Zhang, S. Ding, E. Wang, M. Yan, H. Huang, H. Zhang, Z. Xu, J. Denlinger, A. Fedorov, H. Yang, W. Duan, H. Yao, Y. Wu, S. Fan, H. Zhang, X. Chen, and S. Zhou, *Nat. Phys.* **12**, 1105 (2016).
- [14] A. Crepaldi, G. Autès, G. Gatti, S. Roth, A. Sterzi, G. Manzoni, M. Zacchigna, C. Cacho, R. Chapman, E. Springate, E. A. Seddon, P. Bugnon, H. Magrez, H. Berger, I. Vobornik, M. Kalläne, A. Quer, K. Rossnagel, F. Parmigiani, O. V. Yazyev, and M. Grioni, *Phys. Rev. B* **96**, 241408 (2017).
- [15] E. J. Sie, C. M. Nyby, C. D. Pemmaraju, S. J. Park, X. Shen, J. Yang, M. C. Hoffmann, B. K. Ofori-Okai, R. Li, A. H. Reid, S. Weathersby, E. Mannebach, N. Finney, D. Rhodes, D. Chagnet, A. Antony, L. Balicas, J. Hone, T. P. Devereaux, T. F. Heinz, X. Wang, and A. M. Lindenberg, *Nature* **565**, 61 (2019).
- [16] M. Y. Zhang, Z. X. Wang, Y. N. Li, L. Y. Shi, D. Wu, T. Lin, S. J. Zhang, Y. Q. Liu, Q. M. Liu, J. Wang, T. Dong, and N. L. Wang, *Phys. Rev. X* **9**, 021036 (2019).
- [17] M. Hase, M. Katsuragawa, A. M. Constantinescu, and H. Petek, *Nat. Photonics* **6**, 243 (2012).
- [18] J. D. Hunter, *Computing in Science & Engineering* **9**, 90 (2007).
- [19] K. Ueno, *J. Phys. Soc. Jpn.* **84**, 121015 (2015).
- [20] R. He, S. Zhong, H. H. Kim, G. Ye, Z. Ye, L. Winford, D. McHaffie, I. Rilak, F. Chen, X. Luo, Y. Sun, and A. W. Tsen, *Phys. Rev. B* **97**, 041410 (2018).
- [21] G. Garrett, T. Albrecht, J. Whitaker, and R. Merlin, *Phys. Rev. Lett.* **77**, 3661 (1996).
- [22] T. E. Stevens, J. Kuhl, and R. Merlin, *Phys. Rev. B* **65**, 144304 (2002).
- [23] H. Zeiger, J. Vidal, T. Cheng, E. Ippen, G. Dresselhaus, and M. Dresselhaus, *Phys. Rev. B* **45**, 768 (1992).
- [24] S.-Y. Chen, T. Goldstein, D. Venkataraman, A. Ramasubramaniam, and J. Yan, *Nano Lett.* **16**, 5852 (2016).
- [25] K. Zhang, C. Bao, Q. Gu, X. Ren, H. Zhang, K. Deng, Y. Wu, Y. Li, J. Feng, and S. Zhou, *Nat. Commun.* **7**, 13552 (2016).
- [26] J. Lai, X. Liu, J. Ma, Q. Wang, K. Zhang, X. Ren, Y. Liu, Q. Gu, X. Zhuo, W. Lu, Y. Wu, Y. Li, J. Feng, S. Zhou, J.-H. Chen, and D. Sun, *Adv. Mater.* **30**, 1707152 (2018).
- [27] X. Ma, P. Guo, C. Yi, Q. Yu, A. Zhang, J. Ji, Y. Tian, F. Jin, Y. Wang, K. Liu, T. Xia, Y. Shi, and Q. Zhang, *Phys. Rev. B* **94**, 214105 (2016).
- [28] A. Gambetta, C. Manzoni, E. Menna, M. Meneghetti, G. Cerullo, G. Lanzani, S. Tretiak, A. Piryatinski, A. Saxena, R. L. Martin, and B. A. R, *Nat. Phys.* **2**, 515 (2006).
- [29] J. Li, J. Chen, D. A. Reis, S. Fahy, and R. Merlin, *Phys. Rev. Lett.* **110**, 047401 (2013).
- [30] M. Hase, M. Kitajima, S.-i. Nakashima, and K. Mizoguchi, *Phys. Rev. Lett.* **88**, 067401 (2002).
- [31] M. Hase, P. Fons, K. Mitrofanov, A. V. Kolobov, and J. Tominaga, *Nat. Commun.* **6**, 8367 (2015).
- [32] J. Flock, T. Dekorsy, and O. V. Misochko, *Appl. Phys. Lett.* **105**, 011902 (2014).
- [33] B. He, C. Zhang, W. Zhu, Y. Li, S. Liu, X. Zhu, X. Wu, X. Wang, H.-h. Wen, and M. Xiao, *Sci. Rep.* **6**, 30487 (2016).
- [34] M. Hase, K. Mizoguchi, H. Harima, S.-i. Nakashima, and K. Sakai, *Phys. Rev. B* **58**, 5448 (1998).
- [35] J. Hohlfeld, S.-S. Wellershoff, J. Gädde, U. Conrad, V. Jähnke, and E. Matthias, *Chem. Phys.* **251**, 237 (2000).
- [36] H.-J. Kim, S.-H. Kang, I. Hamada, and Y.-W. Son, *Phys. Rev. B* **95**, 180101 (2017).